

Neutrino Flavor Spin Waves

Huaiyu Duan,^{1,*} George M. Fuller,^{2,†} and Yong-Zhong Qian^{3,‡}

¹*Institute for Nuclear Theory, University of Washington, Seattle, WA 98195*

²*Department of Physics, University of California, San Diego, La Jolla, CA 92093-0319*

³*School of Physics and Astronomy, University of Minnesota, Minneapolis, MN 55455*

Our calculations reveal a collective neutrino flavor transformation phenomenon in supernovae which is closely akin to spin waves in spin lattices. This “neutrino flavor spin wave”, a collective neutrino oscillation mode, can arise in anisotropic neutrino gases because of a symmetry in the equations which govern neutrino flavor evolution. Neutrino flavor transformation with neutrino self-coupling in time-varying, inhomogeneous and anisotropic environments such as supernovae can be described by such flavor spin waves when other non-collective neutrino oscillation modes add up incoherently and average out. We show that the existence of neutrino flavor spin waves in anisotropic environments can explain the stepwise spectral swap (spectral split) phenomenon found in numerical simulations of neutrino flavor transformation in supernovae.

PACS numbers: 14.60.Pq, 97.60.Bw

I. INTRODUCTION

It is well known that neutrino flavor refractive indices can be modified by neutrino forward scattering on ordinary matter [1] as well as by neutrino-neutrino forward scattering [2, 3, 4, 5]. The former gives rise to the Mikheyev-Smirnov-Wolfenstein (MSW) effect in the presence of ordinary matter [1, 6, 7], and the latter can lead to collective neutrino oscillations in astrophysical environments with large neutrino number densities such as the early universe (e.g., Refs. [8, 9, 10, 11]).

Neutrinos can also experience collective flavor transformation in core-collapse supernovae. Unlike the early universe, the supernova environment is highly inhomogeneous and anisotropic because all neutrinos are emitted from a proto-neutron star at the center of the supernova. All early studies adopted the so-called “single-angle approximation” [2, 4, 12, 13, 14, 15, 16]. In this approximation, the flavor evolution histories of all neutrinos with energy E are taken to be the same as those of neutrinos with the same energy E but propagating along a “representative” trajectory, usually taken to be the radial trajectory. Apart from an angle-averaged, effective neutrino number density, this approximation essentially treats supernova neutrinos as homogeneous and isotropic neutrino gases.

Single-angle approximation-based arguments have been employed to show that large-scale collective neutrino oscillations could occur in the dense supernova environment despite the small measured neutrino mass-squared differences [16, 17]. Detailed single-angle numerical simulations [18, 19, 20, 21] reveal that collective neutrino oscillations can leave a unique “fossil” imprint on the energy spectra of supernova neutrinos, the

so-called “stepwise spectral swapping” or the “spectral split”. Both refer to the same phenomenon: neutrinos of different flavors (partly) swap their energy spectra during collective flavor transformation in a manner such that the final neutrino energy spectra exhibit sharp step-like structures. Stepwise spectral swapping in the single-angle approximation has been understood as the result of the “collective precession mode” of neutrino oscillations [18, 22]. This collective mode corresponds to an adiabatic solution to the neutrino flavor evolution equations [23, 24, 25].

Simulations of supernova neutrino flavor transformation with a “multi-angle” treatment have been carried out recently [18, 19, 20]. Compared to the single-angle approximation, this multi-angle treatment more accurately models the anisotropic nature of the supernova environment by simultaneously following the flavor evolution histories of neutrinos propagating along various trajectories. These multi-angle calculations render results which are qualitatively similar to those in the single-angle calculations. In particular, the final neutrino energy spectra in multi-angle calculations also exhibit step-like structures.

Since the discovery of the stepwise spectral swapping phenomenon, a series of papers have discussed collective neutrino flavor transformation and its consequences [20, 21, 22, 23, 24, 25, 26, 27, 28, 29, 30, 31, 32, 33, 34, 35, 36, 37, 38, 39, 40]. However, the stepwise spectral phenomenon in multi-angle simulations is still unexplained and the robustness of this phenomenon in real supernova environments is yet to be confirmed. In fact, it has been shown that collective neutrino oscillations of the bipolar type can experience “kinematic de-coherence” and be disrupted in anisotropic environments [27]. Additionally, a large matter background can result in neutrino oscillation phase differences between different neutrino trajectories in an anisotropic neutrino gas [13], and this effect recently has been shown to result in suppression of collective neutrino oscillations [39]. These results point up the inadequacy of the single-angle approximation in

*Electronic address: Huaiyu.Duan@mailaps.org

†Electronic address: gfuller@ucsd.edu

‡Electronic address: qian@physics.umn.edu

some supernova environments. We note that the current multi-angle treatment of neutrino flavor transformation assumes a spherically symmetric model of the supernova. Removing this symmetry would present a great challenge to numerical computations. It is so far unclear whether the assumed spherical symmetry plays any important role in the results of current multi-angle calculations.

The ultimate solution to the supernova neutrino flavor evolution problem hangs on the resolution of two additional issues. First is the question of the efficacy of the Schrödinger-like mean field treatment of neutrino self-coupling [41, 42, 43]. Second is the effect of turbulence, the supernova shock wave, and small-scale density fluctuations on neutrino flavor evolution [44, 45, 46, 47, 48].

In this paper we will show that a neutrino flavor spin wave can exist in time-varying, inhomogeneous and anisotropic environments. This flavor spin wave corresponds to the collective precession mode of neutrino oscillations. In Sec. II we will show that there exists a special symmetry in the flavor evolution equations of a dense neutrino gas. This symmetry leads to the conservation of neutrino lepton numbers. In Sec. III we will show that neutrino flavor spin waves can arise as a result of the symmetry. We will show that this is true for both the two-flavor and three-flavor mixing schemes. In Sec. IV we will elucidate the neutrino flavor spin wave phenomenon by using results of new multi-angle simulation of supernova neutrino flavor transformation. We will give criteria for determining whether or not a neutrino participates in collective oscillations. In Sec. V we give our conclusions.

II. NEUTRINO FLAVOR EVOLUTION EQUATIONS

A. Neutrino flavor matrix

We are interested in collective neutrino oscillations in dense neutrino gases. When physical conditions change only slowly with spatial dimension, the flavor content of neutrinos can be described by semi-classical flavor density matrices $\rho_p(t, \mathbf{x})$ [49, 50]. Here we use 4-component vector

$$p = [\pm|\mathbf{p}|, \mathbf{p}] \quad (1)$$

to denote a neutrino momentum mode at location \mathbf{x} , where \mathbf{p} is the momentum of the neutrino, and the plus and minus signs are for neutrinos and antineutrinos, respectively. The diagonal elements of $\rho_p(t, \mathbf{x})$ give the occupation numbers of the neutrino eigenstates in a particular basis, and the off-diagonal elements of the matrices contain additional phase information related to neutrino flavor mixing.

In the limit that neutrinos experience only coherent elastic scattering on background neutrinos and other particles, the neutrino flavor density matrices $\rho_p(t, \mathbf{x})$ obey

the equations of motion (e.o.m.) [49, 50, 51]

$$\partial_t \rho_p(t, \mathbf{x}) + \hat{\mathbf{p}} \cdot \nabla \rho_p(t, \mathbf{x}) = -i[H_p(t, \mathbf{x}), \rho_p(t, \mathbf{x})], \quad (2)$$

where $H_p(t, \mathbf{x})$ is the Hamiltonian that governs the flavor evolution of neutrinos, and $\hat{\mathbf{p}} \equiv \mathbf{p}/|\mathbf{p}|$ is the unit vector along the neutrino propagation direction. In Eq. (2) we have ignored the effects of external macroscopic forces such as gravitational deflection and redshift. As in most of the literature on neutrino oscillations, we assume that neutrinos travel with the speed of light c . (Here we use natural units with $\hbar = c = 1$.) We also assume a vanishing CP -violating phase. (See Ref. [40] for a discussion of collective neutrino oscillations with a non-vanishing CP -violation phase.)

When there is no source or sink for neutrinos, the number of neutrinos in each mode p is conserved:

$$\partial_t n_p(t, \mathbf{x}) + \hat{\mathbf{p}} \cdot \nabla n_p(t, \mathbf{x}) = 0, \quad (3)$$

where

$$n_p(t, \mathbf{x}) \equiv \text{Tr} \rho_p(t, \mathbf{x}) \quad (4)$$

is the summed number density of neutrinos of all flavors in momentum mode p at instant t and location \mathbf{x} . The relation in Eq. (3) can be shown easily by taking the trace of the both sides of Eq. (2). Therefore, we can define a new traceless “flavor matrix”

$$P_p(t, \mathbf{x}) \equiv \begin{cases} n_p^{-1}(t, \mathbf{x}) \rho_p(t, \mathbf{x}) - N_f^{-1} \mathbf{1} & \text{if } p^0 > 0, \\ -n_p^{-1}(t, \mathbf{x}) \rho_p(t, \mathbf{x}) + N_f^{-1} \mathbf{1} & \text{if } p^0 < 0, \end{cases} \quad (5)$$

where $\mathbf{1}$ is the identity matrix in flavor space, $N_f = 2$ and 3 for two-flavor and three-flavor mixing schemes, respectively, and p^0 is the time component of the 4-component vector p . The e.o.m. for flavor matrix $P_p(t, \mathbf{x})$ are similar to Eq. (2) and are given by

$$\partial_t P_p(t, \mathbf{x}) + \hat{\mathbf{p}} \cdot \nabla P_p(t, \mathbf{x}) = -i[H_p(t, \mathbf{x}), P_p(t, \mathbf{x})]. \quad (6)$$

The Hamiltonian

$$H_p(t, \mathbf{x}) = H_p^{\text{vac}} + H^{\text{matt}}(t, \mathbf{x}) + H_p^{\nu\nu}(t, \mathbf{x}) \quad (7)$$

has three components that can be viewed as three fields. The Hamiltonian for the “vacuum field”

$$H_p^{\text{vac}} = \frac{M^2}{2p^0} \quad (8)$$

generates vacuum oscillations, where M is the neutrino mass matrix. Because the trace of a Hamiltonian has no effect on neutrino oscillations, we will take H_p^{vac} to be traceless hereafter.

The Hamiltonian for the “matter field” in the *flavor basis* in the supernova environment (however, see Ref. [31]) is

$$H^{\text{matt}}(t, \mathbf{x}) = \sqrt{2} G_F n_e(t, \mathbf{x}) \text{diag}[1, 0, 0], \quad (9)$$

where G_F is the Fermi constant, and $n_e(t, \mathbf{x})$ is the net electron number density.

The Hamiltonian for the background “neutrino field” is

$$H_{\hat{\mathbf{p}}}^{\nu\nu}(t, \mathbf{x}) = \sqrt{2}G_F \sum_{p'} (1 - \hat{\mathbf{p}} \cdot \hat{\mathbf{p}}') n_{p'}(t, \mathbf{x}) P_{p'}(t, \mathbf{x}), \quad (10)$$

where we use $\sum_{p'}$ to denote the integration over $(p')^0$ and $\hat{\mathbf{p}}'$:

$$\sum_{p'} \equiv \int_{-\infty}^{\infty} d(p')^0 \int d\hat{\mathbf{p}}'. \quad (11)$$

The procedure implied in Eq. (11) is tantamount to a sum over neutrino and antineutrino energies and trajectory directions. We note that $H_{\hat{\mathbf{p}}}^{\nu\nu}$ depends only on the propagation direction $\hat{\mathbf{p}}$ but not p^0 of the neutrino or antineutrino under investigation.

B. Conservation of neutrino lepton numbers

In the two-flavor neutrino mixing scheme the vacuum field is

$$H_p^{\text{vac}} = -\frac{\Delta m^2 \sigma_3}{2p^0} \frac{\sigma_3}{2} \quad (12)$$

in the *vacuum mass basis*, where $\Delta m^2 = m_2^2 - m_1^2$ is the mass-squared difference between mass eigenstates $|\nu_2\rangle$ and $|\nu_1\rangle$, and σ_i ($i = 1, 2, 3$) are the Pauli matrices. As noted above, we have ignored the trace term in H_p^{vac} because it does not contribute to neutrino oscillations.

In the absence of ordinary matter [i.e., $H^{\text{matt}}(t, \mathbf{x}) = 0$], Eq. (6) is invariant under the transformation

$$P_p(t, \mathbf{x}) \rightarrow P'_p(t, \mathbf{x}) \equiv U P_p(t, \mathbf{x}) U^\dagger, \quad (13)$$

where

$$U \equiv \exp\left(i\phi \frac{\sigma_3}{2}\right) \quad (14)$$

is a constant, unitary transformation with an arbitrary phase ϕ . This symmetry in the neutrino flavor evolution equations corresponds to the conservation of “neutrino lepton number” in the *vacuum mass basis*. This conservation law can be shown as follows. From Eqs. (6), (10) and (12) we have

$$\sum_p n_p(t, \mathbf{x}) (\partial_t + \hat{\mathbf{p}} \cdot \nabla) \text{Tr}[\sigma_3 P_p(t, \mathbf{x})] = 0. \quad (15)$$

Combining Eqs. (3) and (15) we obtain the conservation law

$$\partial_t n_L(t, \mathbf{x}) + \nabla \cdot \mathbf{J}_L(t, \mathbf{x}) = 0, \quad (16)$$

where

$$n_L(t, \mathbf{x}) \equiv \sum_p n_p(t, \mathbf{x}) \text{Tr}[\sigma_3 P_p(t, \mathbf{x})] \quad (17)$$

is the neutrino lepton number density in the vacuum mass basis (defined as the difference between the net number densities of ν_1 and ν_2), and

$$\mathbf{J}_L(t, \mathbf{x}) \equiv \sum_p \hat{\mathbf{p}} n_p(t, \mathbf{x}) \text{Tr}[\sigma_3 P_p(t, \mathbf{x})] \quad (18)$$

is the associated current vector.

The conservation of neutrino lepton number was first discussed in Ref. [26] for the case of uniform and isotropic neutrino gases. This conservation law follows simply from the assumptions that there is no ordinary matter background and that neutrino-neutrino forward scattering is coherent. We note that neutrino-neutrino forward scattering can exchange the flavors of two intersecting neutrinos. However, the total number of neutrinos in each flavor (or vacuum mass eigenstate) is not changed by this kind of scattering process. Additionally, H_p^{vac} cannot change the number of neutrinos in each vacuum mass eigenstate. As a result, in the absence of ordinary matter, the total number of neutrinos in each vacuum mass eigenstate must be conserved, as is their difference. The continuity equation (3) follows from this conservation law.

The vacuum field in the three-flavor mixing scheme is

$$H_p^{\text{vac}} = -\frac{\Delta m_{21}^2 \lambda_3}{2p^0} \frac{\lambda_3}{2} - \left(\frac{\Delta m_{31}^2 + \Delta m_{32}^2}{4p^0} \right) \frac{\lambda_8}{\sqrt{3}}, \quad (19)$$

where λ_i ($i = 1, 2, \dots, 8$) are the Gell-Mann matrices. Similar to two-flavor mixing scenarios, Eq. (6) is invariant under the transformation in Eq. (13) in the absence of ordinary matter, where now

$$U \equiv \exp\left(i\phi_3 \frac{\lambda_3}{2} + i\phi_8 \frac{\lambda_8}{2}\right) \quad (20)$$

with ϕ_3 and ϕ_8 being two arbitrary, constant phases. Accordingly, there exist two lepton conservation laws

$$\partial_t n_{L,3}(t, \mathbf{x}) + \nabla \cdot \mathbf{J}_{L,3}(t, \mathbf{x}) = 0, \quad (21a)$$

$$\partial_t n_{L,8}(t, \mathbf{x}) + \nabla \cdot \mathbf{J}_{L,8}(t, \mathbf{x}) = 0, \quad (21b)$$

where

$$n_{L,i}(t, \mathbf{x}) \equiv \sum_p n_p(t, \mathbf{x}) \text{Tr}[\lambda_i P_p(t, \mathbf{x})], \quad (22a)$$

$$\mathbf{J}_{L,i}(t, \mathbf{x}) \equiv \sum_p \hat{\mathbf{p}} n_p(t, \mathbf{x}) \text{Tr}[\lambda_i P_p(t, \mathbf{x})]. \quad (22b)$$

C. Neutrino flavor isospin

For two-flavor mixing, the flavor matrix $P_p(t, \mathbf{x})$ can be represented by spin vector¹

$$\vec{s}_p(t, \mathbf{x}) \equiv \frac{1}{2} \text{Tr}[\vec{\sigma} P_p(t, \mathbf{x})] \quad (23)$$

in flavor space. This is the neutrino flavor isospin (NFIS) vector introduced in Ref. [17]. The NFIS notation is similar to the widely-used polarization vector notation [49], except for a sign difference for antineutrinos and a factor of $\frac{1}{2}$ difference in magnitude for both neutrinos and antineutrinos. The sign difference for antineutrinos arises from the σ_2 -transformation for the wavefunctions for antiparticles.

The e.o.m. for NFIS $\vec{s}_p(t, \mathbf{x})$ is

$$(\partial_t + \hat{\mathbf{p}} \cdot \nabla) \vec{s}_p(t, \mathbf{x}) = \vec{s}_p(t, \mathbf{x}) \times \vec{H}_p(t, \mathbf{x}). \quad (24)$$

Eq. (24) shows that NFIS $\vec{s}_p(t, \mathbf{x})$ precesses around the total effective field

$$\vec{H}_p(t, \mathbf{x}) \equiv -\text{Tr}[\vec{\sigma} H_p], \quad (25a)$$

$$= \vec{H}_p^{\text{vac}} + \vec{H}_p^{\text{matt}}(t, \mathbf{x}) + \sum_{p'} \mu_{\hat{\mathbf{p}}, \hat{\mathbf{p}}'} n_{p'}(t, \mathbf{x}) \vec{s}_{p'}(t, \mathbf{x}) \quad (25b)$$

with angular frequency $|\vec{H}_p(t, \mathbf{x})|$, where

$$\mu_{\hat{\mathbf{p}}, \hat{\mathbf{p}}'} \equiv -2\sqrt{2}G_F(1 - \hat{\mathbf{p}} \cdot \hat{\mathbf{p}}') \quad (26)$$

is the ‘‘spin-spin coupling’’. Here $\vec{H}_p^{\text{vac}} + \vec{H}_p^{\text{matt}}(t, \mathbf{x})$ can be regarded as the ‘‘external field’’ for NFIS $\vec{s}_p(t, \mathbf{x})$.

III. FLAVOR SPIN WAVES AND ADIABATIC/PRECESSION SOLUTIONS

A. Planar flavor spin waves

Because of the special symmetry in the neutrino flavor evolution equations in the absence of ordinary matter (see Sec. II B), there can exist neutrino flavor spin waves in dense neutrino gases. We can illustrate the general idea of neutrino flavor spin waves using a simple example. Consider, for example, a planar neutrino flavor spin wave in a two-flavor, homogeneous but anisotropic neutrino gas. In this example, we assume that neutrinos are emitted from an infinitely large plane \mathcal{S} at $z = 0$ into the right half-space ($z > 0$). We further assume that the

emitted neutrino number flux n_p for any neutrino momentum mode p is invariant across plane \mathcal{S} and does not vary with time. As far as the neutrino number densities are concerned, the neutrino gas in the right half-space is indeed homogeneous, and the number density of any neutrino momentum mode p is n_p [see Fig. 1(a)]. Note that this neutrino gas is also isotropic in the case where n_p does not depend on momentum mode direction $\hat{\mathbf{p}}$.

In the absence of ordinary matter, it will prove convenient to work in the vacuum mass basis. We adopt this basis throughout Sec. III unless otherwise stated. With $n_e = 0$, the e.o.m. for the NFIS’s are invariant under the rotation of the whole system around axis

$$\hat{e}_3 \equiv \frac{\vec{H}_p^{\text{vac}}}{|\vec{H}_p^{\text{vac}}|} \quad (27)$$

through an arbitrary angle in flavor space. Here \hat{e}_i ($i = 1, 2, 3$) are the vacuum-mass-basis unit vectors in flavor space. This is identical to the symmetry that follows from the invariance of the neutrino flavor evolution equations under the constant unitary transformation in Eq. (13). As shown in Sec. II B, this symmetry corresponds to the conservation of the neutrino lepton number which, in the NFIS notation, is

$$\sum_p (\partial_t + \hat{\mathbf{p}} \cdot \nabla) [n_p(t, \mathbf{x}) s_{p,3}(t, \mathbf{x})] = 0, \quad (28)$$

where

$$s_{p,i}(t, \mathbf{x}) \equiv \vec{s}_p(t, \mathbf{x}) \cdot \hat{e}_i, \quad i = 1, 2, 3. \quad (29)$$

The neutrino flavor distribution and evolution in the right half-space is completely determined by the e.o.m. of the NFIS’s [Eq. (24)] and the boundary conditions on plane \mathcal{S} . Here we will specify these boundary conditions by assuming that the neutrino flavor distribution on plane \mathcal{S} is homogeneous at $t = 0$:

$$\vec{s}_p(0, \mathbf{x}) = \vec{s}_p(0, \mathbf{0}) \quad (30)$$

for $\mathbf{x} \in \mathcal{S}$. We further will assume that at $t = 0$ each NFIS on plane \mathcal{S} precesses steadily around \hat{e}_3 in flavor space as the corresponding neutrino propagates along its world line. With these specifications, and at instant $t = 0$, the time evolution of the NFIS’s on plane \mathcal{S} is described by

$$(\partial_t + \hat{\mathbf{p}} \cdot \nabla) \vec{s}_p(t, \mathbf{x}) = \vec{s}_p(t, \mathbf{x}) \times (-\Omega + \hat{\mathbf{p}} \cdot \mathbf{K}) \hat{e}_3 \quad (31)$$

for $\mathbf{x} \in \mathcal{S}$. In Eq. (31) Ω is a constant number, and \mathbf{K} is a constant vector in the same or opposite direction to the z axis:

$$\mathbf{K} = (\mathbf{K} \cdot \hat{\mathbf{z}}) \hat{\mathbf{z}}, \quad (32)$$

where $\hat{\mathbf{z}}$ is a unit vector in the direction of the z axis in coordinate space.

¹ We have adopted the convention in Ref. [38]. We use bold-faced letters (e.g., \mathbf{p}) to denote 3-vectors in coordinate space, sans-serif letters (e.g., \mathbf{H}) for operators in flavor space, and letters with an arrow (e.g., \vec{s}) for vectors in flavor space.

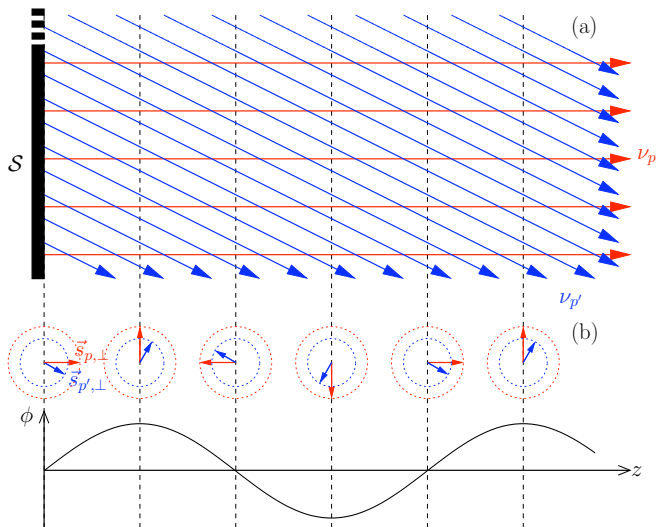


FIG. 1: (Color online) (a) Schematic plot of the fluxes for two neutrino momentum modes p and p' . Neutrino number densities to the right of plane \mathcal{S} are homogeneous ($\nabla n_p(\mathbf{x}) = \nabla n_{p'}(\mathbf{x}) = \mathbf{0}$) but not isotropic ($n_p \neq n_{p'}$). (b) In a flavor spin wave solution the perpendicular components ($\vec{s}_{p,\perp}$ and $\vec{s}_{p',\perp}$) of the NFIS's precess at the same rate in the \hat{e}_1 - \hat{e}_2 plane of flavor space. The differences between the azimuthal angles of the NFIS's and the phase ϕ of the wave do not change with time or location.

It is important to point out that \mathbf{K} in Eq. (31) cannot be just any vector. From Eqs. (24) and (31) we have

$$\vec{s}_p(0, \mathbf{x}) \times \vec{\tilde{H}}_p(0, \mathbf{x}) = 0 \quad (33)$$

for $\mathbf{x} \in \mathcal{S}$, where

$$\vec{\tilde{H}}_p(0, \mathbf{x}) = \vec{H}_p(0, \mathbf{x}) + (\Omega - \hat{\mathbf{p}} \cdot \mathbf{K})\hat{e}_3. \quad (34)$$

In other words, on plane \mathcal{S} , NFIS $\vec{s}_p(0, \mathbf{x})$ is either aligned or antialigned with $\vec{\tilde{H}}_p(0, \mathbf{x})$ in flavor space:

$$\vec{s}_p(0, \mathbf{x}) = \frac{\epsilon_p}{2} \frac{\vec{\tilde{H}}_p(0, \mathbf{x})}{|\vec{\tilde{H}}_p(0, \mathbf{x})|}, \quad (35)$$

where $\epsilon_p = +1$ for alignment and -1 for antialignment. Given values for $[\Omega, n_p, \epsilon_p, n_L]$ at $t = 0$ and $\mathbf{x} = 0$, Eqs. (17) and (35) can be solved for $[\mathbf{K} \cdot \hat{\mathbf{z}}, \vec{s}_p(0, \mathbf{0})]$.

Unlike \mathbf{K} , the components of $\vec{s}_p(0, \mathbf{0})$ actually cannot be uniquely determined from Eqs. (17) and (35) alone. This is because the e.o.m. for the NFIS's are invariant under the simultaneous rotation of all NFIS's around \hat{e}_3 by an arbitrary angle. If the NFIS's $\vec{s}_p(0, \mathbf{0})$ satisfy Eqs. (17) and (35), so do the NFIS's that have been simultaneously rotated around \hat{e}_3 by an arbitrary angle relative to $\vec{s}_p(0, \mathbf{0})$. This arbitrariness can be eliminated by fixing the azimuthal angle of any single NFIS in the \hat{e}_1 - \hat{e}_2 plane of flavor space.

We will assume that all NFIS's $\vec{s}_p(t, \mathbf{x})$ on \mathcal{S} precess simultaneously in flavor space around \hat{e}_3 with the same rate Ω . This gives the time dependence of the NFIS's on plane \mathcal{S} :

$$\partial_t \vec{s}_p(t, \mathbf{x}) = \vec{s}_p(t, \mathbf{x}) \times (-\Omega \hat{e}_3). \quad (36)$$

At instant t , each NFIS $\vec{s}_p(t, \mathbf{x})$ on plane \mathcal{S} has rotated in flavor space around \hat{e}_3 by angle Ωt relative to $\vec{s}_p(0, \mathbf{x})$. Using our assumption that the neutrino flavor distribution on plane \mathcal{S} is homogeneous at $t = 0$, we can conclude this distribution is homogeneous at any subsequent instant t . In addition, because of the invariance of the e.o.m. of the NFIS's under simultaneous rotation around \hat{e}_3 in flavor space, Eq. (31) is valid for any NFIS $\vec{s}_p(t, \mathbf{x})$ on plane \mathcal{S} at any instant t .

Consider a NFIS $\vec{s}_p(t', \mathbf{x}')$ at $t' = t + \delta t$ and $\mathbf{x}' = \mathbf{x} + \delta \mathbf{x}$, where δt and $\delta \mathbf{x}$ are the temporal and spatial intervals along the world line of the corresponding neutrino. According to the above discussion, NFIS $\vec{s}_p(t', \mathbf{x}')$ has rotated around \hat{e}_3 by an angle

$$\phi(t', z') = \Omega t + (\Omega \delta t - \mathbf{K} \cdot \delta \mathbf{x}), \quad (37a)$$

$$= \Omega t' - (\mathbf{K} \cdot \hat{\mathbf{z}})z' \quad (37b)$$

relative to $\vec{s}_p(0, \mathbf{x}) = \vec{s}_p(0, \mathbf{0})$, where $z' = \mathbf{x}' \cdot \hat{\mathbf{z}}$. Clearly this result is independent of the neutrino momentum mode p . A NFIS in any momentum mode p' on plane \mathcal{S}' at $z = z'$ and at instant t' must have rotated by the same angle $\phi(t', z')$ relative to NFIS $\vec{s}_{p'}(0, \mathbf{0})$. This means that the neutrino flavor distribution on plane \mathcal{S}' , like that on plane \mathcal{S} , is also homogeneous and varies with time according to Eq. (36). Further, because the e.o.m. of NFIS's are invariant under the simultaneous rotation of all the NFIS's around \hat{e}_3 in flavor space, the NFIS's on plane \mathcal{S}' must also precess around \hat{e}_3 in flavor space as described by Eq. (31) as the corresponding neutrinos propagate along their world lines. The two planes \mathcal{S} and \mathcal{S}' are, therefore, equivalent in this sense. Using the neutrino flavor distribution and evolution on plane \mathcal{S}' as the beginning boundary condition, we can repeat the argument given above and thereby reach similar conclusions for the NFIS's on plane \mathcal{S}'' at $z = z' + \delta z$. Repeating this procedure, we can conclude that, at any instant t and location \mathbf{x} , NFIS $\vec{s}_p(t, \mathbf{x})$ is the same as $\vec{s}_p(0, \mathbf{0})$ but has rotated around \hat{e}_3 by angle $\phi(t, z) = \Omega t - (\mathbf{K} \cdot \hat{\mathbf{z}})z$.

With our adopted boundary conditions on plane \mathcal{S} [Eqs. (30), (31) and (36)], we can now see that the solution to the neutrino flavor evolution equations is a planar neutrino flavor spin wave that travels with velocity

$$\mathbf{v} = \frac{\Omega}{\mathbf{K} \cdot \hat{\mathbf{z}}} \hat{\mathbf{z}}. \quad (38)$$

The wave fronts are planes that are parallel to \mathcal{S} . The phase function of the wave is $\phi(t, z)$.

This neutrino flavor spin wave corresponds to the collective precession mode for neutrino oscillations. In this collective mode, when neutrinos propagate along their world lines from one wave front of the flavor spin wave to

another, the corresponding NFIS's rotate around \hat{e}_3 by a common angle in flavor space [see Fig. 1(b)].

B. Flavor spin waves in inhomogeneous and anisotropic neutrino gases

Neutrino self-coupling can allow neutrino flavor spin waves to exist in dense, inhomogeneous and anisotropic neutrino gases. This can be true if the properties of the neutrino gas vary only slowly with space and time. If this is the case, in small local regions and for short durations, flavor spin waves can be approximated as the plane waves described in Sec. III A.

It is convenient to study the evolution of the NFIS's

in a special set of ‘‘corotating frames’’ [17]. The basis vectors $\hat{e}_i(t, \mathbf{x})$ for one of these frames at instant t and location \mathbf{x} are the same as the vacuum-mass-basis unit vectors \hat{e}_i , but have been rotated around \hat{e}_3 by angle $\phi(t, \mathbf{x})$, where $\phi(t, \mathbf{x})$ is the phase function of the neutrino flavor spin wave. The total effective field experienced by NFIS $\vec{s}_p(t, \mathbf{x})$ in this corotating frame is

$$\tilde{\vec{H}}_p(t, \mathbf{x}) \equiv \vec{H}_p(t, \mathbf{x}) + [\partial_t \phi(t, \mathbf{x}) - \hat{\mathbf{p}} \cdot \nabla \phi(t, \mathbf{x})] \hat{e}_3. \quad (39)$$

According to the discussion in Sec. III A, NFIS $\vec{s}_p(t, \mathbf{x})$ is approximately static in this corotating frame and is either aligned or antialigned with $\tilde{\vec{H}}_p(t, \mathbf{x})$. Using this result, in component form NFIS $\tilde{\vec{H}}_p(t, \mathbf{x})$ is

$$s_{p,\perp}(t, \mathbf{x}) \cos \varphi_p \simeq \frac{\epsilon_p(t, \mathbf{x})}{2|\tilde{\vec{H}}_p(t, \mathbf{x})|} \sum_{p'} \mu_{\hat{\mathbf{p}} \cdot \hat{\mathbf{p}}'} n_{p'} s_{p',\perp}(t, \mathbf{x}) \cos \varphi_{p'}, \quad (40a)$$

$$\tilde{s}_{p,\perp}(t, \mathbf{x}) \sin \varphi_p \simeq \frac{\epsilon_p(t, \mathbf{x})}{2|\tilde{\vec{H}}_p(t, \mathbf{x})|} \sum_{p'} \mu_{\hat{\mathbf{p}} \cdot \hat{\mathbf{p}}'} n_{p'} s_{p',\perp}(t, \mathbf{x}) \sin \varphi_{p'}, \quad (40b)$$

$$s_{p,3}(t, \mathbf{x}) \simeq \frac{\epsilon_p(t, \mathbf{x})}{2|\tilde{\vec{H}}_p(t, \mathbf{x})|} [\omega_p + (\partial_t - \hat{\mathbf{p}} \cdot \nabla) \phi(t, \mathbf{x}) + \sum_{p'} \mu_{\hat{\mathbf{p}} \cdot \hat{\mathbf{p}}'} n_{p'} s_{p',3}(t, \mathbf{x})], \quad (40c)$$

where subscript ‘‘ \perp ’’ denotes the projection of a vector in the \hat{e}_1 - \hat{e}_2 plane, $\epsilon_p(t, \mathbf{x}) = +1$ (-1) if $\vec{s}_p(t, \mathbf{x})$ is aligned (antialigned) with $\tilde{\vec{H}}_p(t, \mathbf{x})$, φ_p is the azimuthal angle of $\vec{s}_p(t, \mathbf{x})$ in the *corotating frame* in flavor space, and

$$\omega_p \equiv \frac{\Delta m^2}{2p^0} \quad (41)$$

is the vacuum oscillation frequency.

We note that φ_p does not vary with time or space. If this were not the case, the precession in flavor space of the NFIS's for different momentum modes would not be coherent, and the collective neutrino flavor oscillation would break down. However, it is generally impossible to find $s_{p,\perp}(t, \mathbf{x})$ for all momentum modes and for space-time coordinates that satisfy both Eqs. (40a) and (40b) unless all the NFIS's lie within the same azimuthal plane:

$$\varphi_p = \varphi^{(0)} + l_p \pi, \quad l_p = 0 \text{ or } 1. \quad (42)$$

We can redefine $\phi_p(t, \mathbf{x})$ in such a way that $\varphi^{(0)} = 0$. We also can define

$$\tilde{s}_{p,1}(t, \mathbf{x}) \equiv \vec{s}_p(t, \mathbf{x}) \cdot \hat{e}_1(t, \mathbf{x}), \quad (43a)$$

$$= (-1)^{l_p} s_{p,\perp}(t, \mathbf{x}), \quad l_p = 0 \text{ or } 1 \quad (43b)$$

to be the first component of NFIS $\vec{s}_p(t, \mathbf{x})$ in the *corotating frame* in flavor space. Eq. (40b) is now trivially

satisfied and Eq. (40a) becomes

$$\tilde{s}_{p,1}(t, \mathbf{x}) \simeq \frac{\epsilon_p(t, \mathbf{x})}{2|\tilde{\vec{H}}_p(t, \mathbf{x})|} \sum_{p'} \mu_{\hat{\mathbf{p}} \cdot \hat{\mathbf{p}}'} n_{p'} \tilde{s}_{p',1}(t, \mathbf{x}). \quad (44)$$

We also note that the alignment factor $\epsilon_p(t, \mathbf{x})$ for NFIS $\vec{s}_p(t, \mathbf{x})$ should be constant along the corresponding neutrino's world line:

$$(\partial_t + \hat{\mathbf{p}} \cdot \nabla) \epsilon_p(t, \mathbf{x}) = 0. \quad (45)$$

With specified boundary conditions, Eqs. (3) and (45) can be solved for $[n_p(t, \mathbf{x}), \epsilon_p(t, \mathbf{x})]$. Eqs. (28), (40c) and (44) then can be solved for $[\phi(t, \mathbf{x}), \tilde{s}_{p,1}(t, \mathbf{x}), s_{p,3}(t, \mathbf{x})]$.

The NFIS distribution $\vec{s}_p(t, \mathbf{x})$ calculated in this way describes a flavor spin wave in the time-varying, inhomogeneous and anisotropic neutrino gas. This flavor spin wave corresponds to the collective precession mode for neutrino oscillations. This is a natural generalization of the two-flavor adiabatic/precession solution for the neutrino flavor evolution in a homogeneous and isotropic environment [23]. In reality, neutrino flavor evolution does not follow exactly the adiabatic/precession solution because $\tilde{\vec{H}}_p(t, \mathbf{x})$ may rotate in the \hat{e}_1 - \hat{e}_3 plane. However, if $\tilde{\vec{H}}_p(t, \mathbf{x})$ varies slowly with time and space such that

$$\frac{|(\partial_t + \hat{\mathbf{p}} \cdot \nabla) \vartheta_p(t, \mathbf{x})|}{|\tilde{\vec{H}}_p(t, \mathbf{x})|} \ll 1, \quad (46)$$

NFIS $\vec{s}_p(t, \mathbf{x})$ will follow closely the rotation of $\tilde{\vec{H}}_p(t, \mathbf{x})$. Here

$$\vartheta_p(t, \mathbf{x}) \equiv \arccos \left(\frac{\tilde{\vec{H}}_p(t, \mathbf{x}) \cdot \hat{e}_3}{|\tilde{\vec{H}}_p(t, \mathbf{x})|} \right) \quad (47)$$

is the polar angle of $\tilde{\vec{H}}_p(t, \mathbf{x})$ relative to \hat{e}_3 . The flavor distribution and evolution of the neutrino system is well approximated by the adiabatic/precession solution whenever Eq. (46) is satisfied for all neutrino modes and at any time and for any location.

C. Flavor matrix description of the adiabatic/precession solution

It is useful to recast the equations for the two-flavor adiabatic/precession solution in the flavor matrix description. Following Ref. [25], we will demand that an adiabatic/precession solution satisfy two conditions, the ‘‘precession ansatz’’ and the ‘‘adiabatic ansatz’’.

As in Sec. III B, we will work in the corotating frames which correspond to the unitary transformations:

$$P_p(t, \mathbf{x}) \rightarrow \tilde{P}_p(t, \mathbf{x}) \equiv U(t, \mathbf{x})P_p(t, \mathbf{x})U^\dagger(t, \mathbf{x}), \quad (48)$$

where

$$U_p(t, \mathbf{x}) \equiv \exp \left[i\phi(t, \mathbf{x}) \frac{\sigma_3}{2} \right] \quad (49)$$

with $\phi(t, \mathbf{x})$ being the phase function for the flavor spin wave. Using Eqs. (6) and (48) we have

$$(\partial_t + \hat{\mathbf{p}} \cdot \nabla) \tilde{P}_p(t, \mathbf{x}) = -i[\tilde{H}_p(t, \mathbf{x}), \tilde{P}_p(t, \mathbf{x})], \quad (50)$$

where

$$\begin{aligned} \tilde{H}_p(t, \mathbf{x}) &\equiv U(t, \mathbf{x})H_p(t, \mathbf{x})U^\dagger(t, \mathbf{x}) \\ &\quad - \frac{\sigma_3}{2}(\partial_t + \hat{\mathbf{p}} \cdot \nabla)\phi(t, \mathbf{x}), \\ &= -[\omega_p + (\partial_t + \hat{\mathbf{p}} \cdot \nabla)\phi(t, \mathbf{x})] \frac{\sigma_3}{2} \\ &\quad + \sqrt{2}G_F \sum_{p'} (1 - \hat{\mathbf{p}} \cdot \hat{\mathbf{p}}') n_{p'}(t, \mathbf{x}) P_{p'}(t, \mathbf{x}) \end{aligned} \quad (51a)$$

$$(51b)$$

is the total effective field experienced by the neutrino in momentum mode p in the *corotating frame*.

The *precession ansatz* is that, in the corotating frame determined by $\phi(t, \mathbf{x})$, the flavor matrix for each neutrino mode is approximately static along the neutrino’s world line:

$$[\tilde{H}_p(t, \mathbf{x}), \tilde{P}_p(t, \mathbf{x})] \simeq 0. \quad (52)$$

For the pure collective precession mode for neutrino oscillations, we note that, in the corotating frame, there must be no extra precession generated by σ_3 :

$$\text{Tr}\{\sigma_3 [\tilde{P}_p(t, \mathbf{x}), (\partial_t + \hat{\mathbf{p}} \cdot \nabla)\tilde{P}_p(t, \mathbf{x})]\} = 0. \quad (53)$$

Clearly, the $\tilde{P}_p(t, \mathbf{x})$ components are overconstrained by Eqs. (52) and (53) because the number of unknowns is less than the number of equations. In Sec. III B we stipulated that all NFIS’s had to lie in the \hat{e}_1 – \hat{e}_3 plane. In the flavor matrix description, this corresponds to the requirement that $\tilde{P}_p(t, \mathbf{x})$ are always real:

$$\text{Tr}[\sigma_2 \tilde{P}_p(t, \mathbf{x})] = 0. \quad (54)$$

In this case, Eq. (53) is trivially satisfied, and we need to find real symmetric matrices $\tilde{P}_p(t, \mathbf{x})$ that satisfy Eq. (52). Because real symmetric matrices $\tilde{H}_p(t, \mathbf{x})$ and $\tilde{P}_p(t, \mathbf{x})$ commute with each other, they can be diagonalized by the same orthogonal matrix $X_p(t, \mathbf{x})$:

$$X_p(t, \mathbf{x})\tilde{H}_p(t, \mathbf{x})X_p^T(t, \mathbf{x}) = -\tilde{\omega}_p(t, \mathbf{x}) \frac{\sigma_3}{2}, \quad (55a)$$

$$X_p(t, \mathbf{x})\tilde{P}_p(t, \mathbf{x})X_p^T(t, \mathbf{x}) = \epsilon_p(t, \mathbf{x}) \frac{\sigma_3}{2}, \quad (55b)$$

where $\tilde{\omega}_p(t, \mathbf{x}) > 0$, and $\epsilon_p(t, \mathbf{x}) = \pm 1$.

The *adiabatic ansatz* is that the probability for a neutrino mode to be in each particular instantaneous mass state in the corotating frame is constant along the neutrino’s world line [Eq. (45)].

With specified boundary conditions, Eqs. (3) and (45) can be solved for $[n_p(t, \mathbf{x}), \epsilon_p(t, \mathbf{x})]$. The procedure outlined in Ref. [25] then can be followed to solve Eqs. (16) and (52) for $[\phi(t, \mathbf{x}), \tilde{P}_p(t, \mathbf{x})]$.

It is now straightforward to generalize the equations for the adiabatic/precession solution to the three-flavor mixing case. This can be done using the flavor matrix formalism [25]. Because the e.o.m. for $P_p(t, \mathbf{x})$ are invariant under the simultaneous SU(3) rotation generated by λ_3 and λ_8 , we expect that there exist two independent phase functions $\phi_3(t, \mathbf{x})$ and $\phi_8(t, \mathbf{x})$ for flavor spin waves. We require the precession ansatz in Eq. (52) to hold, but with Eqs. (49) and (51) replaced by

$$U_p(t, \mathbf{x}) \equiv \exp \left[i\phi_3(t, \mathbf{x}) \frac{\lambda_3}{2} + i\phi_8(t, \mathbf{x}) \frac{\lambda_8}{2} \right] \quad (56)$$

and

$$\begin{aligned} \tilde{H}_p(t, \mathbf{x}) &\equiv U(t, \mathbf{x})H_p(t, \mathbf{x})U^\dagger(t, \mathbf{x}) \\ &\quad - (\partial_t + \hat{\mathbf{p}} \cdot \nabla) \left[\phi_3(t, \mathbf{x}) \frac{\lambda_3}{2} + \phi_8(t, \mathbf{x}) \frac{\lambda_8}{2} \right], \end{aligned} \quad (57)$$

respectively.

For a pure collective precession, there must be no extra rotation in the corotating frame that is generated by λ_3 or λ_8 :

$$\text{Tr}\{\lambda_3 [\tilde{P}_p(t, \mathbf{x}), (\partial_t + \hat{\mathbf{p}} \cdot \nabla)\tilde{P}_p(t, \mathbf{x})]\} = 0, \quad (58a)$$

$$\text{Tr}\{\lambda_8 [\tilde{P}_p(t, \mathbf{x}), (\partial_t + \hat{\mathbf{p}} \cdot \nabla)\tilde{P}_p(t, \mathbf{x})]\} = 0. \quad (58b)$$

Therefore, the components of $\tilde{P}_p(t, \mathbf{x})$ are overconstrained by Eqs. (52) and (58). As in the two-flavor mixing scenario, we demand that the components of $\tilde{P}_p(t, \mathbf{x})$

be real:

$$\text{Tr}[\lambda_2 \tilde{\mathbf{P}}_p(t, \mathbf{x})] = \text{Tr}[\lambda_5 \tilde{\mathbf{P}}_p(t, \mathbf{x})] = \text{Tr}[\lambda_7 \tilde{\mathbf{P}}_p(t, \mathbf{x})] = 0. \quad (59)$$

The constraints in Eq. (58) are now trivially satisfied.

Because real symmetric matrices $\tilde{\mathbf{H}}_p(t, \mathbf{x})$ and $\tilde{\mathbf{P}}_p(t, \mathbf{x})$ commute with each other, they can be diagonalized by the same orthogonal matrix $\mathbf{X}_p(t, \mathbf{x})$:

$$\mathbf{X}_p(t, \mathbf{x}) \tilde{\mathbf{H}}_p(t, \mathbf{x}) \mathbf{X}_p^T(t, \mathbf{x}) = \text{diag}[\tilde{\omega}^L, \tilde{\omega}^M, \tilde{\omega}^H]_p(t, \mathbf{x}), \quad (60a)$$

$$\mathbf{X}_p(t, \mathbf{x}) \tilde{\mathbf{P}}_p(t, \mathbf{x}) \mathbf{X}_p^T(t, \mathbf{x}) = \text{diag}[\tilde{g}^L, \tilde{g}^M, \tilde{g}^H]_p(t, \mathbf{x}), \quad (60b)$$

where $\tilde{\omega}_p^L(t, \mathbf{x}) \leq \tilde{\omega}_p^M(t, \mathbf{x}) \leq \tilde{\omega}_p^H(t, \mathbf{x})$. The adiabatic ansatz requires that

$$(\partial_t + \hat{\mathbf{p}} \cdot \nabla) \tilde{g}_p^l(t, \mathbf{x}) = 0, \quad l = L, M, H. \quad (61)$$

With specified boundary conditions, Eqs. (3) and (61) can be solved for $[n_p(t, \mathbf{x}), \tilde{g}_p^l(t, \mathbf{x})]$. Subsequently, Eqs. (21) and (52) can be solved for $[\phi_3(t, \mathbf{x}), \phi_8(t, \mathbf{x}), \tilde{\mathbf{P}}_p(t, \mathbf{x})]$. This gives the three-flavor adiabatic/precession solution.

D. Effects of ordinary matter

Although we have assumed that $\mathbf{H}^{\text{matt}}(t, \mathbf{x}) = 0$ in the above discussions, neutrino flavor spin waves can exist even in the presence of a large matter background:

$$|\mathbf{H}^{\text{matt}}(t, \mathbf{x})| \gg |\mathbf{H}_p^{\text{vac}}|. \quad (62)$$

Here the norm of a traceless Hermitian matrix \mathbf{A} is defined as

$$|\mathbf{A}| \equiv [\text{Tr}(\mathbf{A}^2)]^{1/2}. \quad (63)$$

We can decompose the vacuum field $\mathbf{H}_p^{\text{vac}}$ as a sum of two orthogonal components:

$$\mathbf{H}_p^{\text{vac}} = \mathbf{H}_{p,\parallel}^{\text{vac}} + \mathbf{H}_{p,\perp}^{\text{vac}} \quad (64)$$

with

$$|\mathbf{H}_p^{\text{vac}}|^2 = |\mathbf{H}_{p,\parallel}^{\text{vac}}|^2 + |\mathbf{H}_{p,\perp}^{\text{vac}}|^2. \quad (65)$$

Here $\mathbf{H}_{p,\parallel}^{\text{vac}}$ is the component of the vacuum field that is “parallel” to the matter field

$$[\mathbf{H}^{\text{matt}}(t, \mathbf{x}), \mathbf{H}_{p,\parallel}^{\text{vac}}] = 0, \quad (66)$$

but also has the maximum size. By maximum size, we mean the largest possible value of $|\mathbf{H}_{p,\parallel}^{\text{vac}}|$. In Eq. (64) $\mathbf{H}_{p,\perp}^{\text{vac}}$ is the “perpendicular” component of the vacuum field which satisfies

$$\text{Tr}[\mathbf{H}^{\text{matt}}(t, \mathbf{x}) \mathbf{H}_{p,\perp}^{\text{vac}}] = 0. \quad (67)$$

The effects of $\mathbf{H}_{p,\perp}^{\text{vac}}$ become negligible when Eq. (62) is valid [17, 25]. In this case, the above discussions about

the adiabatic/precession solution still apply, but with the replacement

$$\mathbf{H}_p^{\text{vac}} \longrightarrow \mathbf{H}_{p,\parallel}^{\text{vac}} + \mathbf{H}^{\text{matt}}(t, \mathbf{x}). \quad (68)$$

For two-flavor mixing scenarios, we can follow the same procedure as outlined in Sec. III B if we substitute the *flavor basis* for the vacuum mass basis and we identify

$$\omega_p \longrightarrow \omega_p^{\text{matt}}(t, \mathbf{x}) \equiv \omega_p \cos 2\theta_v - \lambda(t, \mathbf{x}), \quad (69)$$

where θ_v is the effective vacuum mixing angle, and

$$\lambda(t, \mathbf{x}) \equiv \sqrt{2} G_F n_e(t, \mathbf{x}). \quad (70)$$

IV. NEUTRINO FLAVOR SPIN WAVES IN SUPERNOVAE

A. Collective precession mode

As a relevant example we consider two-flavor collective neutrino oscillations in supernovae. We have performed new multi-angle simulations for the flavor transformation of supernova neutrinos. These simulations are similar to those described in Refs. [18, 19] but calculate neutrino flavor evolution at much later supernova epochs. We assume that the neutrinos are emitted from a thin sphere (i.e., the “neutrino sphere”) with radius $R = 10$ km. In these calculations we also assume the emission of neutrinos to be uniform across the neutrino sphere with energy luminosity $L_\nu = 10^{50}$ erg/s for each neutrino species. We approximate the neutrino energy spectra at the neutrino sphere with a two-parameter Fermi-Dirac form:

$$f_\nu(E) = \frac{1}{T_\nu^3 F_2(\eta_\nu)} \frac{E^2}{\exp(E/T_\nu - \eta_\nu) + 1}, \quad (71)$$

where

$$F_k(\eta) = \int_0^\infty \frac{\xi^k d\xi}{\exp(\xi - \eta) + 1}. \quad (72)$$

We take $\eta_\nu = 3$ to be the same for all neutrino species, and choose T_ν to be such that the average energies for various neutrino species are $\langle E_{\nu_e} \rangle = 10$ MeV, $\langle E_{\bar{\nu}_e} \rangle = 12$ MeV, and $\langle E_{\nu_x} \rangle = \langle E_{\bar{\nu}_x} \rangle = 13$ MeV, respectively. Here $|\nu_x\rangle$ ($|\bar{\nu}_x\rangle$) corresponds to an approximate linear combination of $|\nu_\mu\rangle$ and $|\nu_\tau\rangle$ ($|\bar{\nu}_\mu\rangle$ and $|\bar{\nu}_\tau\rangle$). We take the effective vacuum mixing angle to be $\theta_v = 0.1$, and the mass-squared difference to be $\Delta m^2 = -3 \times 10^{-3} \text{ eV}^2$ (inverted neutrino mass hierarchy). Note that in the effective 2×2 mixing scheme which we employed $\theta_v \simeq \theta_{13}$ and $|\Delta m^2|$ is approximately the atmospheric neutrino mass-squared difference Δm_{atm}^2 [52].

We adopt a simple analytical profile for the electron number density:

$$n_e(r) = (9.2 \times 10^{30} \text{ cm}^{-3}) \left(\frac{100}{S}\right)^4 \left(\frac{10 \text{ km}}{r}\right)^3, \quad (73)$$

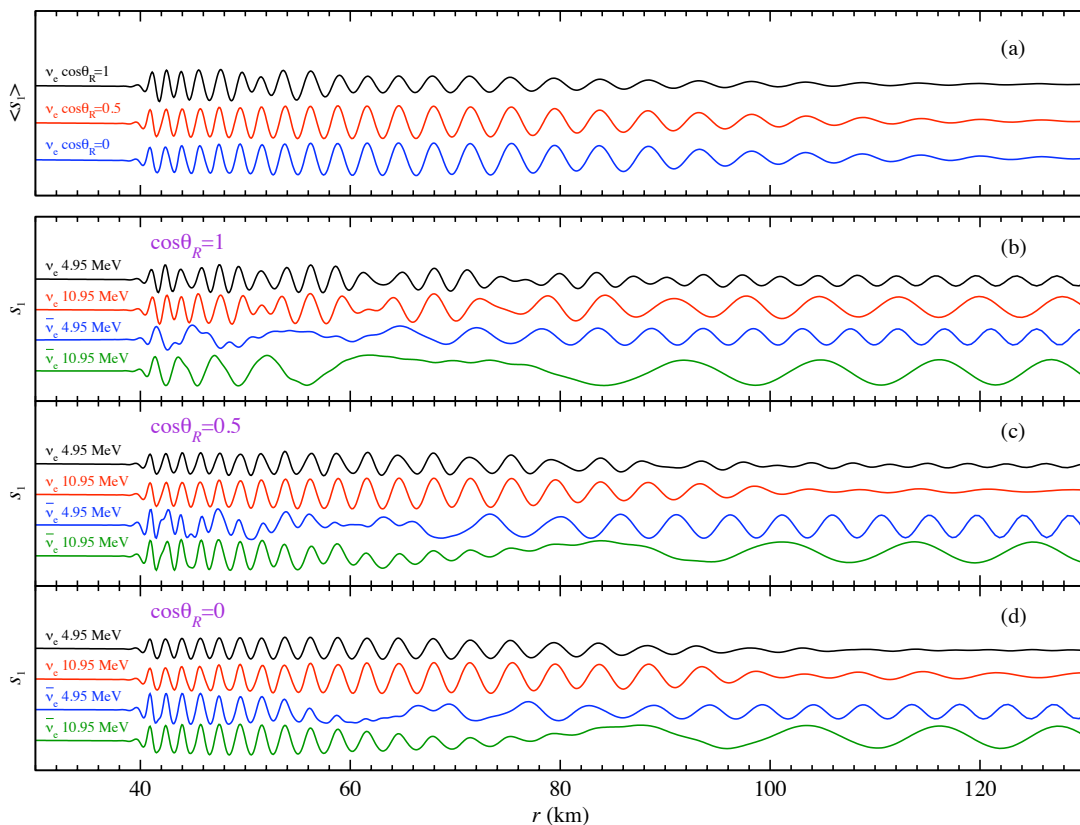


FIG. 2: (Color online) Oscillations of $s_1(r)$, the projection of the NFIS on \hat{e}_1 , as functions of r . The curves in the top panel are for neutrinos emitted as ν_e and propagating along trajectories with $\cos\theta_R = 1, 0.5$ and 0 , respectively. Here $\langle s_1 \rangle$ represents an average over the initial ν_e energy spectrum. The curves in the bottom panels show s_1 for individual energy and angle bins (as labelled). The neutrinos or antineutrinos corresponding to these curves start as pure ν_e or $\bar{\nu}_e$ as labelled. Note that the NFIS's for both neutrinos and antineutrinos precess with a common frequency at modest radius but precess with energy-dependent vacuum oscillation frequencies at large radius. Additionally, the NFIS's for antineutrinos precess in opposite direction from neutrinos at large radius (not shown).

where r is the distance to the center of the proto-neutron star, and the density profile is parametrized by S , the entropy per baryon in units of Boltzmann's constant k_B . In the simulation we discuss here we take $S = 250$.

Compared to the parameters employed in the simulations presented in Ref. [18], these new calculations use neutrino energy spectra which have less disparity between the various neutrino species. Consequently, in these new calculations collective neutrino oscillations can arise at larger neutrino fluxes [17]. In addition, our new calculations employ a smaller neutrino luminosity. Because neutrino fluxes decrease with r , in these calculations we expect collective neutrino oscillations to arise much closer to the neutrino sphere than in previous simulations. We note that the single-angle approximation cannot be used to follow collective neutrino oscillations near the neutrino sphere where the neutrino propagation directions are very different and where the differences between various neutrino trajectories can be significant.

In Fig. 2(a) we plot $\langle s_1(r) \rangle$, the energy-averaged NFIS component $s_1(r) \equiv \vec{s}_p(r) \cdot \hat{e}_1$, as functions of r for neu-

trinos emitted as pure ν_e and propagating along a few representative trajectories. We here do not distinguish between vacuum mass and flavor bases because $\theta_v \ll 1$. Because of our assumed spherical symmetry, it suffices to label different neutrino trajectories by neutrino emission angle θ_R , which can be defined to be

$$\cos\theta_r(\hat{\mathbf{p}}) \equiv \hat{\mathbf{p}} \cdot \hat{\mathbf{r}} \quad (74)$$

evaluated at $r = R$, with $\hat{\mathbf{r}}$ being the radial direction.

In Fig. 2(a) we observe that $\langle s_1(r) \rangle$ for various neutrino trajectories oscillates along r in phase at $r \gtrsim 40$ km. This is a clear signature of neutrino flavor transformation in the collective precession mode, and can be explained as follows. Because we have assumed a time-independent configuration, our discussions in Sec. III would indicate that we should expect a standing flavor spin wave in our simulations of the flavor transformation of supernova neutrinos. Because of the assumed spherical symmetry in our supernova model, the phase $\phi(r)$ of this flavor spin wave should depend only on radius r . This flavor spin wave corresponds to the collective precession mode of

neutrino oscillations, and $\phi(r)$ is the common azimuthal angle of all the NFIS's in flavor space.

According to the discussions in Sec. III B, if a neutrino participates in the collective precession mode, its flavor evolution approximately follows the adiabatic/precession solution, and the corresponding NFIS $\vec{s}_p(r)$ is aligned or antialigned with

$$\vec{H}_p(r) \simeq [\omega_p^{\text{matt}}(r) + K(r) \cos \theta_r] \hat{e}_3 - \vec{\Sigma}_{\theta_r}(r), \quad (75)$$

where

$$K(r) \equiv -\frac{d}{dr} \phi(r), \quad (76)$$

and

$$\vec{\Sigma}_{\theta_r(\hat{\mathbf{p}})}(r) \equiv 2\sqrt{2}G_{\text{F}} \sum_{p'} (1 - \hat{\mathbf{p}} \cdot \hat{\mathbf{p}}') n_{p'}(r) \vec{s}_{p'}(r). \quad (77)$$

From Eq. (75) we can see that NFIS $\vec{s}_p(r)$ will be approximately aligned or antialigned with \hat{e}_3 if

$$|\omega_p^{\text{matt}}(r) + K(r) \cos \theta_r| \gtrsim |\vec{\Sigma}_{\theta_r}(r)|. \quad (78)$$

In other words, neutrino flavor transformation in the collective precession mode is suppressed if Eq. (78) holds for most neutrinos.

When local neutrino fluxes are negligible, as the neutrino moves along its world line the corresponding NFIS $\vec{s}_p(r)$ will precess around \hat{e}_3 with angular velocity $-\omega_p^{\text{matt}}(r)$. On the other hand, when local neutrino fluxes are large, NFIS $\vec{s}_p(r)$ will experience a strong field $\vec{\Sigma}_{\theta_r}(r)$ generated by all the other NFIS's. In this case, NFIS $\vec{s}_p(r)$ instead will precess around \hat{e}_3 with angular velocity $K(r) \cos \theta_r$. Clearly, the larger the difference between $-\omega_p^{\text{matt}}(r)$ and $K(r) \cos \theta_r$, the stronger will be the field $\vec{\Sigma}_{\theta_r}(r)$ required for $\vec{s}_p(r)$ to participate in collective precession. Therefore, Eq. (78) serves as a criterion to determine whether local neutrino fluxes at r are too small for neutrino mode p to participate in the collective precession mode.

In Figs. 2(b-d) we plot $s_1(r)$ for a dozen individual angular and energy bins for both neutrinos and antineutrinos. These figures illustrate the breakdown of the collective precession mode. We can see from these figure that the NFIS's for most of the neutrinos precess along r in phase in the immediate region above $r \simeq 40$ km. This corresponds to neutrino flavor transformation in the collective precession mode. As local neutrino fluxes decrease with r , the NFIS's gradually drop out of the collective precession mode. At $r \gtrsim 100$ km both neutrino fluxes and the matter density are low, and the NFIS's precess roughly with their individual energy-dependent vacuum oscillation frequencies.

There are two important trends in the breakdown of the collective precession mode which merit further elaboration. One of these trends is that along each neutrino trajectory antineutrinos always drop out of the collective

mode earlier than do neutrinos, and antineutrinos with smaller energies drop out earlier than those with larger energies.

This trend can be explained by using the criterion in Eq. (78). We note that the collective oscillation frequency $K(r)$ is an average of the intrinsic frequencies of all neutrino momentum modes:

$$K(r) \simeq \langle \omega_p \rangle_p - \lambda(r), \quad (79)$$

where we have assumed $\cos \theta_r \simeq 1$. This is a good approximation when r is at least a few times larger than R . We note that ω_p will have a different sign for neutrinos and antineutrinos. For the inverted neutrino mass hierarchy ($\Delta m^2 < 0$), we have $\omega_p < 0$ for neutrinos and $\omega_p > 0$ for antineutrinos. Therefore, we expect the momentum mode average $\langle \omega_p \rangle_p$ to satisfy $\langle \omega_p \rangle_p < 0$. This is because in our case there are more neutrinos than antineutrinos. For neutrinos and antineutrinos propagating along the same trajectory,

$$|\omega_p^{\text{matt}}(r) + K(r) \cos \theta_r| \simeq |\omega_p - \langle \omega_{p'} \rangle_{p'}| \quad (80)$$

is larger for antineutrinos than for neutrinos. Therefore, Eq. (78) is satisfied at smaller radii for antineutrinos than for neutrinos. In addition, the smaller the energy of the antineutrino, the earlier Eq. (78) will be satisfied, and, of course, at smaller r the antineutrinos drop out of the collective oscillation mode.

The second trend is that neutrinos or antineutrinos propagating along the radial trajectory ($\cos \theta_R = 1$) drop out of the collective precession mode earlier than do those with the same energies but propagating along the tangential trajectory ($\cos \theta_R = 0$). This can also be explained by Eq. (78). For our spherically symmetric supernova model, Eq. (77) can be written as [18]

$$\vec{\Sigma}_{\theta_r}(r) = \frac{\sqrt{2}G_{\text{F}}}{\pi R^2} \int_{\cos \theta_r^{\text{max}}}^1 d(\cos \theta'_r) (1 - \cos \theta_r \cos \theta'_r) \times \sum_{\nu} \frac{L_{\nu}}{\langle E_{\nu} \rangle} \int_0^{\infty} dE f_{\nu}(E) \vec{s}_{\nu, \theta'_r, E}(r), \quad (81)$$

where

$$\cos \theta_r^{\text{max}} = \sqrt{1 - \left(\frac{R}{r}\right)^2}, \quad (82)$$

and where the summation is over all neutrino and antineutrino species. Assuming that $\vec{s}_{\nu, \theta_r, E}$ does not vary too much with θ_r , we expect $|\vec{\Sigma}_{\theta_r}(r)|$ to achieve a minimum for the radial trajectory ($\theta_r = \theta_R = 0$) and to increase with θ_r or θ_R . Therefore, neutrinos and antineutrinos propagating along the radial trajectory will satisfy Eq. (78) before other neutrinos and, as a result, will drop out of the collective precession mode first.

B. Stepwise spectral swapping

After they stream out of the region where neutrino flavor spin waves exist, neutrinos of different flavors can

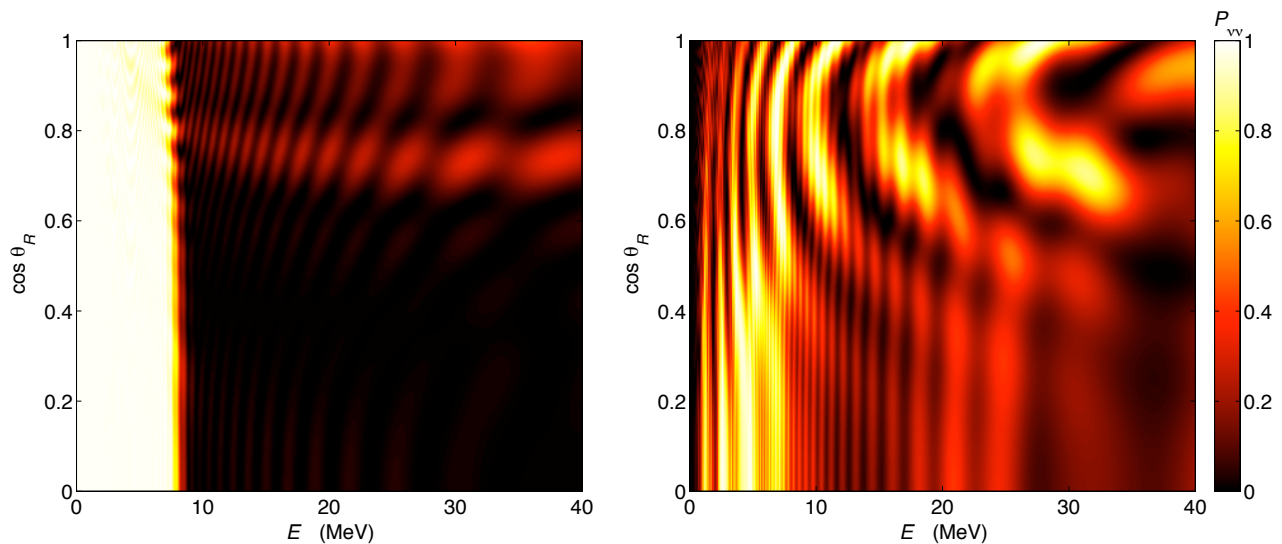


FIG. 3: (Color online) The neutrino survival probabilities $P_{\nu\nu}(E, \theta_R)$ as functions of neutrino energy E and emission angle θ_R at $r = 200$ km. The left panel is for neutrinos and the right panel is for antineutrinos. Shading code for $P_{\nu\nu}(E, \theta_R)$ is given at right.

swap portions of their energy spectra. In fact, the neutrino survival probability $P_{\nu\nu}(E)$ can be approximately a step function of neutrino energy E , changing from almost no flavor conversion to almost complete flavor conversion within a narrow energy range. This phenomenon, dubbed “stepwise spectral swapping” or the “spectral split”, was discovered in the calculations reported in Ref. [18, 19].

Stepwise swapping of neutrino energy spectra is a result of the collective precession of NFIS’s as was first pointed out in Ref. [18]. If a neutrino participates in the collective precession mode, the corresponding NFIS $\vec{s}_p(r)$ is either aligned or antialigned with $\vec{H}_p(r)$ [see Eq. (75)]. This alignment or antialignment does not change with radius. When the NFIS breaks away from the collective precession [Eq. (78)], we will have

$$\vec{s}_p(r) \simeq \frac{\epsilon_p}{2} \text{sgn}(\omega_p^{\text{matt}}(r) + K(r) \cos \theta_r) \hat{e}_3, \quad (83)$$

where $\epsilon_p = +1$ (-1) if $\vec{s}_p(r)$ is aligned (antialigned) with $\vec{H}_p(r)$ during collective precession. In the NFIS notation, a neutrino (antineutrino) is a pure ν_e ($\bar{\nu}_x$) if the corresponding NFIS \vec{s}_p is aligned with \hat{e}_3 , and is a pure ν_x ($\bar{\nu}_e$) if \vec{s}_p is antialigned with \hat{e}_3 . Therefore, if all NFIS’s participate in collective precession out to large enough distance from the proto-neutron star that both neutrino and matter backgrounds are negligible, we expect

$$P_{\nu\nu}(E) \simeq \begin{cases} 1 & \text{for neutrinos with } E < E^s, \\ 0 & \text{for neutrinos with } E > E^s. \\ 0 & \text{for antineutrinos} \end{cases} \quad (84)$$

for the calculations we have performed. Note that the behavior of $P_{\nu\nu}(E)$ will be opposite ($P_{\nu\nu}(E) = 0$ for $E <$

E^s and $P_{\nu\nu}(E) = 1$ for $E > E^s$) if we have adopted the normal mass hierarchy instead of the inverted mass hierarchy. In Eq. (84)

$$E^s = \left. \frac{\Delta m^2}{2K(r)} \right|_{r \rightarrow \infty} \quad (85)$$

is the critical energy at which neutrinos of different flavors swap their energy spectra. This result is the same as the prediction based on the single-angle approximation.

In Fig. 3 we plot survival probabilities $P_{\nu\nu}(E, \theta_R)$ as functions of both neutrino energy E and emission angle θ_R for both neutrinos and antineutrinos. We observe that the results in Fig. 3 agree with Eq. (84) reasonably well. However, because neutrinos and antineutrinos actually drop out of collective oscillations at finite distances from the proto-neutron star, the numerical results presented in Fig. 3 are different from the simplistic prediction of Eq. (84) in some important details.

One of these details is that the simplistic prescription in Eq. (84) works better for neutrinos than for antineutrinos. In fact, this prescription breaks down for antineutrinos with energies ~ 5 MeV and/or those propagating along the radial trajectory. This is because the difference between $-\omega_p^{\text{matt}}(r)$ and $K(r) \cos \theta_r$ is larger for antineutrinos than for neutrinos. Therefore, antineutrinos participate in collective oscillations to a less extent than neutrinos do (see Sec. IV A and Fig. 2), and the predictions based on the pure collective precession mode are not as accurate for antineutrinos as they are for neutrinos. In particular, antineutrinos with energies $E \lesssim 0.8$ MeV do not participate in collective oscillations at all and are almost fully converted through the MSW mechanism. Antineutrinos with energies $E \sim 5$ MeV do participate

in collective oscillations. However, they encounter MSW resonances after their leave the collective precession mode and, as a result, are (partly) converted back to their original flavors.

Another important detail is that the critical energy E^s is actually different for neutrinos propagating along different trajectories. This difference has two main contributions. The first contribution stems from the fact that the collective precession frequency $K(r) \cos \theta_r$ along a neutrino world line depends on the neutrino propagation direction. It is the largest along the radial trajectory and the smallest along the tangential trajectory. The second contribution arises because neutrinos propagating along different trajectories drop out of the collective precession mode at different radii. Neutrinos propagating along more radially-directed trajectories stop participating in collective oscillations at smaller distances from the proto-neutron star, but neutrinos propagating along more tangential trajectories stay in collective oscillations out to larger distances. Our numerical calculations show that the collective precession frequency always decreases as neutrino fluxes decrease. Therefore, both contributions lead to a smaller E^s for the radial trajectory and a larger E^s for the tangential trajectory. Indeed, the left panel of Fig. 3 shows that E^s for the radial and tangential trajectories differ by ~ 0.7 MeV.

C. Suppression of collective oscillations by ordinary matter

Ref. [13] showed that the matter background can produce significant neutrino oscillation phase differences between different neutrino trajectories in an anisotropic neutrino gas. Ref. [39] has recently shown that this effect results in suppression of large-scale collective neutrino flavor transformation in the presence of a very large matter background. This can be understood using Eq. (78) as follows.

For a dominant matter background we have

$$\lambda(r) \gg |\omega_p| \quad (86)$$

for most neutrinos. For this case, collective neutrino flavor transformation will be dominated by precession around the matter field, and

$$\lambda(r) \lesssim K(r) \lesssim \frac{\lambda(r)}{\cos \theta_r^{\max}}. \quad (87)$$

As a rough estimate we can take

$$K(r) \simeq \frac{\lambda(r)}{2} \left(1 + \frac{1}{\cos \theta_r^{\max}} \right). \quad (88)$$

For the radial trajectory we then have

$$|\omega_p^{\text{matt}}(r) + K(r) \cos \theta_r| \simeq \frac{\sqrt{2}G_F}{4} \left(\frac{R}{r} \right)^2 n_e(r) \quad (89)$$

for $r \gg R$. On the other hand, if we assume that all neutrinos are in their initial flavors, we would have

$$|\vec{\Sigma}_{\theta_r=0}| \simeq \frac{\sqrt{2}G_F}{16\pi R^2} \frac{\epsilon L_{\nu_e}}{\langle E_{\nu_e} \rangle} \left(\frac{R}{r} \right)^4 \quad (90)$$

for $r \gg R$, where

$$\epsilon \equiv 1 - \frac{L_{\bar{\nu}_e}/\langle E_{\bar{\nu}_e} \rangle}{L_{\nu_e}/\langle E_{\nu_e} \rangle} \quad (91)$$

is a measure of the difference between the number fluxes of ν_e and $\bar{\nu}_e$ at the neutrino sphere. Using Eqs. (78), (89) and (90), we find that neutrinos propagating along the radial trajectory will not participate in the collective precession mode when

$$n_e(r) \gtrsim \frac{\epsilon L_{\nu_e}}{4\pi r^2 \langle E_{\nu_e} \rangle}, \quad (92)$$

or, equivalently,

$$\begin{aligned} \rho_{\text{matt}}(r) &\gtrsim (1.4 \times 10^8 \text{ g cm}^{-3}) \left(\frac{0.4}{Y_e} \right) \left(\frac{L_{\nu_e}}{10^{51} \text{ erg s}^{-1}} \right) \\ &\times \left(\frac{\epsilon}{0.2} \right) \left(\frac{10 \text{ MeV}}{\langle E_{\nu_e} \rangle} \right) \left(\frac{10^6 \text{ cm}}{r} \right)^2, \end{aligned} \quad (93)$$

where ρ_{matt} is the matter density, and Y_e is the electron fraction. According to Ref. [17], collective neutrino oscillations cease for locations with

$$\begin{aligned} r &\gtrsim (1.4 \times 10^7 \text{ cm}) \left(\frac{3 \times 10^{-3} \text{ eV}^2}{|\Delta m^2|} \right)^{1/4} \left(\frac{R}{10^6 \text{ cm}} \right)^{1/2} \\ &\times \left(\frac{L_{\nu_e}}{10^{51} \text{ erg s}^{-1}} \right)^{1/4} \left(\frac{\langle E_{\nu_e} \rangle}{\Delta E_{\nu_e}} \right)^{1/4}, \end{aligned} \quad (94)$$

where ΔE_{ν_e} is the width of the ν_e energy distribution at the neutrino sphere. Comparing Eqs. (93) and (94) to typical density profiles for iron core-collapse supernovae (e.g., Fig. 1 in Ref. [53]), we find that collective neutrino oscillations may be suppressed during the first few seconds post-core-bounce.

V. CONCLUSIONS

We have shown that, in the absence of ordinary matter, a special symmetry in the neutrino flavor evolution equations leads to the conservation of neutrino lepton numbers. Because of this symmetry, there can exist a planar flavor spin wave in homogeneous but anisotropic neutrino gases. This flavor spin wave corresponds to the collective precession mode of neutrino oscillations. This collective oscillation mode can exist even in a time-varying, inhomogeneous and anisotropic neutrino system, as long as the system changes slowly with space and time. This is true for both the two-flavor and three-flavor mixing schemes, except that there exist two independent flavor

spin waves in the three-flavor mixing scheme as compared to one spin wave in the two-flavor mixing scheme.

We have proposed a criterion for determining whether or not a neutrino or antineutrino participates in collective oscillations. We have demonstrated that this criterion could be used to explain many important qualitative features in multi-angle simulations of neutrino flavor transformation in supernovae. In particular, we now can understand the stepwise spectral swapping phenomenon observed in multi-angle calculations. The swap phenomenon in multi-angle simulations is similar to the swap calculated in single-angle simulations, but there can be a slight angular dependence in the former case.

We have shown that the collective precession mode for neutrino oscillations can exist even in the presence of a large matter background. (Here by large matter background potentials we mean compared to vacuum potentials.) On the other hand, we also confirm that collective neutrino oscillations can be suppressed in an anisotropic

environment in the presence of a very large matter density [39]. This suppression could occur during the very early post-core-bounce evolution of an iron core-collapse supernova.

Acknowledgments

This work was supported in part by DOE grants DE-FG02-00ER41132 at INT, DE-FG02-87ER40328 at UMN, NSF grant PHY-04-00359 at UCSD, and an IGPP/LANL mini-grant. This research used resources of the National Energy Research Scientific Computing Center, which is supported by the Office of Science of the U.S. Department of Energy under Contract No. DE-AC02-05CH11231. We thank J. Carlson, J. J. Cherry, A. Friedland, W. Haxton, D. B. Kaplan, C. Kishimoto, C. Lunardini and A. Mezzacappa for insightful discussions.

-
- [1] L. Wolfenstein, Phys. Rev. **D17**, 2369 (1978).
 [2] G. M. Fuller, R. W. Mayle, J. R. Wilson, and D. N. Schramm, Astrophys. J. **322**, 795 (1987).
 [3] D. Nötzold and G. Raffelt, Nucl. Phys. **B307**, 924 (1988).
 [4] G. M. Fuller, R. W. Mayle, B. S. Meyer, and J. R. Wilson, Astrophys. J. **389**, 517 (1992).
 [5] J. T. Pantaleone, Phys. Rev. **D46**, 510 (1992).
 [6] L. Wolfenstein, Phys. Rev. **D20**, 2634 (1979).
 [7] S. P. Mikheyev and A. Y. Smirnov, Yad. Fiz. **42**, 1441 (1985), [Sov. J. Nucl. Phys. **42**, 913 (1985)].
 [8] S. Samuel, Phys. Rev. **D48**, 1462 (1993).
 [9] V. A. Kostelecky and S. Samuel, Phys. Rev. **D52**, 621 (1995), hep-ph/9506262.
 [10] S. Samuel, Phys. Rev. **D53**, 5382 (1996), hep-ph/9604341.
 [11] S. Pastor, G. G. Raffelt, and D. V. Semikoz, Phys. Rev. **D65**, 053011 (2002), hep-ph/0109035.
 [12] Y.-Z. Qian, G. M. Fuller, G. J. Mathews, R. W. Mayle, J. R. Wilson, and S. E. Woosley, Phys. Rev. Lett. **71**, 1965 (1993).
 [13] Y. Z. Qian and G. M. Fuller, Phys. Rev. **D51**, 1479 (1995), astro-ph/9406073.
 [14] S. Pastor and G. Raffelt, Phys. Rev. Lett. **89**, 191101 (2002), astro-ph/0207281.
 [15] A. B. Balantekin and H. Yüksel, New J. Phys. **7**, 51 (2005), astro-ph/0411159.
 [16] G. M. Fuller and Y.-Z. Qian, Phys. Rev. **D73**, 023004 (2006), astro-ph/0505240.
 [17] H. Duan, G. M. Fuller, and Y.-Z. Qian, Phys. Rev. **D74**, 123004 (2006), astro-ph/0511275.
 [18] H. Duan, G. M. Fuller, J. Carlson, and Y.-Z. Qian, Phys. Rev. **D74**, 105014 (2006), astro-ph/0606616.
 [19] H. Duan, G. M. Fuller, J. Carlson, and Y.-Z. Qian, Phys. Rev. Lett. **97**, 241101 (2006), astro-ph/0608050.
 [20] G. L. Fogli, E. Lisi, A. Marrone, and A. Mirizzi, JCAP **0712**, 010 (2007), arXiv:0707.1998 [hep-ph].
 [21] H. Duan, G. M. Fuller, J. Carlson, and Y.-Z. Qian, Phys. Rev. Lett. **100**, 021101 (2008), 0710.1271.
 [22] H. Duan, G. M. Fuller, J. Carlson, and Y.-Z. Qian, Phys. Rev. **D75**, 125005 (2007), astro-ph/0703776.
 [23] G. G. Raffelt and A. Y. Smirnov, Phys. Rev. **D76**, 081301(R) (2007), arXiv:0705.1830 [hep-ph].
 [24] G. G. Raffelt and A. Y. Smirnov, Phys. Rev. **D76**, 125008 (2007), arXiv:0709.4641 [hep-ph].
 [25] H. Duan, G. M. Fuller, and Y.-Z. Qian, Phys. Rev. **D77**, 085016 (2008), 0801.1363.
 [26] S. Hannestad, G. G. Raffelt, G. Sigl, and Y. Y. Y. Wong, Phys. Rev. **D74**, 105010 (2006), astro-ph/0608695.
 [27] G. G. Raffelt and G. G. R. Sigl, Phys. Rev. **D75**, 083002 (2007), hep-ph/0701182.
 [28] A. Esteban-Pretel, S. Pastor, R. Tomas, G. G. Raffelt, and G. Sigl, Phys. Rev. **D76**, 125018 (2007), arXiv:0706.2498 [astro-ph].
 [29] H. Duan, G. M. Fuller, and Y.-Z. Qian, Phys. Rev. **D76**, 085013 (2007), arXiv:0706.4293 [astro-ph].
 [30] H. Duan, G. M. Fuller, J. Carlson, and Y.-Z. Qian, Phys. Rev. Lett. **99**, 241802 (2007), arXiv:0707.0290 [astro-ph].
 [31] A. Esteban-Pretel, S. Pastor, R. Tomas, G. G. Raffelt, and G. Sigl, Phys. Rev. **D77**, 065024 (2008), 0712.1137.
 [32] B. Dasgupta and A. Dighe (2007), arXiv:0712.3798 [hep-ph].
 [33] B. Dasgupta, A. Dighe, A. Mirizzi, and G. G. Raffelt, Phys. Rev. **D77**, 113007 (2008), 0801.1660.
 [34] B. Dasgupta, A. Dighe, and A. Mirizzi (2008), 0802.1481.
 [35] H. Duan, G. M. Fuller, and J. Carlson (2008), 0803.3650.
 [36] R. F. Sawyer (2008), 0803.4319.
 [37] S. Chakraborty, S. Choubey, B. Dasgupta, and K. Kar (2008), 0805.3131.
 [38] B. Dasgupta, A. Dighe, A. Mirizzi, and G. G. Raffelt (2008), 0805.3300.
 [39] A. Esteban-Pretel et al. (2008), 0807.0659.
 [40] J. Gava and C. Volpe (2008), 0807.3418.
 [41] N. F. Bell, A. A. Rawlinson, and R. F. Sawyer, Phys. Lett. **B573**, 86 (2003), hep-ph/0304082.
 [42] A. Friedland and C. Lunardini, JHEP **10**, 043 (2003), hep-ph/0307140.
 [43] A. B. Balantekin and Y. Pehlivan, J. Phys. **G34**, 47 (2007), astro-ph/0607527.

- [44] R. F. Sawyer, Phys. Rev. **D42**, 3908 (1990).
- [45] F. N. Loreti, Y. Z. Qian, G. M. Fuller, and A. B. Balantekin, Phys. Rev. **D52**, 6664 (1995), astro-ph/9508106.
- [46] R. C. Schirato and G. M. Fuller (2002), astro-ph/0205390.
- [47] A. Friedland and A. Gruzinov (2006), astro-ph/0607244.
- [48] J. P. Kneller, G. C. McLaughlin, and J. Brockman, Phys. Rev. **D77**, 045023 (2008), arXiv:0705.3835 [astro-ph].
- [49] G. Sigl and G. Raffelt, Nucl. Phys. **B406**, 423 (1993).
- [50] P. Strack and A. Burrows, Phys. Rev. **D71**, 093004 (2005), hep-ph/0504035.
- [51] C. Y. Cardall (2007), arXiv:0712.1188 [astro-ph].
- [52] W.-M. Yao et al., J. Phys. **G33**, 1 (2006).
- [53] R. Tomas et al., JCAP **0409**, 015 (2004), astro-ph/0407132.